ADVANCED FUNCTIONAL MATERIALS
www.afm-journal.de

A Real-Time Imaging Sensing System to Visualize Elastomer Surface Profile Evolution for Dynamic Tactile Recognition

*Zhibin Zou, Zilan Li, Yuanzhi Zhou, Guoyuan Zhou, Weiliang Xu, Muxing Huang, Wenfeng Wu, Huiming Zhang, Zhaohe Dai, and Xinming Li**

Elastomer-based interfaces provide rich functionalities for tactile sensing, particularly in making tiny differences in contact dynamics potentially detectable. However, the minimal motion-induced changes in the elastomer's surface and their disappearance during time-lapse limit the state recognition within the current scheme of motion recognition. In this work, a new scheme of real-time motion mode recognition for subtle deformations is proposed, which uses an optical tactile sensing system to visualize and distinguish tiny variations in surface profile evolution encoded as images. Illustrating with a sphere, sliding-induced asymmetric elastomer surface deformation is visualized as a "drag" in optical images. The convolutional neural network (CNN) algorithm is used to analyze the evolution of surface contour features during the interaction between the sphere and the elastic medium. Motion state recognition is achieved with 80% accuracy when a displacement of only 8.3% of the sphere diameter is produced. In addition, the system also offers the potential to analyze dynamic motion information through a single image, with an accuracy of 82.7% for velocity recognition. This dynamic real-time recognition framework for soft media deformation paves the way for novel motion-based input commands for tactile sensing and human-computer interaction applications.

1. Introduction

The contact perception of the human-computer interface is crucial for the recognition of interactive instructions.[1–5] During the touch process, opportunities for obtaining multi-model contact information arise through the design of interface elastomers, electronic skin, or humanoid dexterous hands.[6–11] Adopting a soft contact interface enables the acquisition of response position and deformation behavior in the contact to enable data richness.[6,12–16] However, existing characterizations of the contact behavior focus on the deformation position and area of the soft interface,[17–19] which are far from sufficient to resolve complex and especially dynamic motion behaviors.[20] For example, the rolling and sliding of the contact on the interface is difficult to recognize. The key reason is that the deformation of elastomers caused by movement behavior is concealment at the microscopic scale, and will fade out with time.[20,21] The loss of such undercover deformation features disables the distinction between slightly different motion behaviors. Therefore, accurately identifying contact behavior requires obtaining micro-deformation of the elastomer surface.[22–28] How to dynamically identify the difference of micro-deformations under different motion behaviors is therefore of great significance and challenges.[29,30]

The detection of elastomer deformations can be realized by the contact model algorithm. The contact behavior of the object causes the elastomer surface to deform, which in turn causes the signal change of the deformation area detection system.[31,32] With the help of the algorithm model, the deformation of the elastomer surface can be reconstructed accurately with high resolution. However, in the deformations analysis method dominated by an algorithm model, the requirement of a tailored contact model for elastomers with varying parameters lacks versatility. Another strategy for detecting deformations is based on optical methods, which allow to recording of contact information as images.[33] For example, binocular vision schemes can be used to characterize and visualize the dynamic 3D distribution of traction stress at a micro-nano scale.[34] Computer vision-based optical strain (CVOS) technology can achieve low hysteresis detection of the tensile behavior of the elastomer surface.[35] In addition, combining the marker array with the finite element analysis method is an effective way to achieve real-time detection of deformations.[36–39] However, the large amount of redundant information in visual imaging systems and the limited density of marker array systems make it not always effective to extract

Z. Zou, Z. Li, Y. Zhou, G. Zhou, W. Xu, M. Huang, W. Wu, H. Zhang, X. Li
Guangdong Provincial Key Laboratory of Nanophotonic Functional Materials and Devices
Guangdong Basic Research Center of Excellence for Structure and Fundamental Interactions of Matter
School of Optoelectronic Science and Engineering
South China Normal University
Guangzhou 510006, China
E-mail: xmli@m.scnu.edu.cn
Z. Dai
Department of Mechanics and Engineering Science
State Key Laboratory for Turbulence and Complex Systems
College of Engineering
Peking University
Beijing 100871, China

The ORCID identification number(s) for the author(s) of this article can be found under https://doi.org/10.1002/adfm.202416731

DOI: 10.1002/adfm.202416731

information about micro-deformations. This makes it difficult to dynamically record and digitize such differences in deformation profiles, hindering the analysis of the object's dynamic contact state.[40]

To address the demand and challenge of dynamic real-time detection of elastomer micro-deformation, this work explores a scheme of real-time deformation recognition using an optical tactile sensing system to visualize and digitize the evolution of the elastomer surface profile during time-lapse, which enables the identification of motion behavior. Taking the analysis of the motion behavior of a sphere as an example, the optical system is used to perform real-time dynamic identification of the tiny deformation of the elastomer caused by the motion of the sphere. The system encodes the tiny deformations of the elastomer surface utilizing optical signals and tiny units of Complementary Metal Oxide Semiconductor (CMOS). The difference in the motion behavior of the sphere is manifested as the different evolution forms of the surface contour of the elastic medium over time and transmitted by a combination of intensity variations in continuous light signals. We used a high-resolution optical perception method to record the surface contour of the elastic medium in the form of an image. Thanks to the advantages of the convolutional neural network algorithm in image feature processing, the motion behavior recognition based on the analysis of the surface contour features of the tiny elastic medium was successfully realized. Taking the motion behavior of the 6 mm diameter sphere as an example, motion state recognition with 80% accuracy is achieved when a displacement of only 8.3% of the sphere diameter is produced. In addition, we have also achieved dynamic motion information analysis through a single image, and the accuracy of motion speed recognition has reached 82.7%. This method has great application potential in tactile sensing that requires real-time dynamic detection and subtle evolution in the surface morphology of the elastomer. A "behavior prediction" scenario is set to demonstrate the system's advantages in detecting the dynamic evolution of subtle motion features. The result helps to understand the dynamic motion occurring on elastomers and hence plays an important role in human-computer interaction platforms.

2. Results and Discussion

2.1. Dynamic Deformation Recognition Scheme Based on Optical Image Representation

Contact of a rigid object with an elastomer will result in deformation of the elastomer related to both the contact behavior and the shape of the object. Therefore, by identifying and resolving the deformation, it is feasible to evaluate the contact behavior. Here, we use a steel sphere as a model object. During the horizontal sliding of the sphere, the increase of the lateral contact region will raise the shear forces, which is like the ploughing effect in metallic friction.[22,40,41] This directly changes the distribution of the horizontal contact stresses p_{x1} and p_{x2} on both sides and the vertical contact stress p_z. As a consequence, asymmetric deformation of the elastomer is eventually developed under the action of contact stress. In contrast, this phenomenon is not obvious in the rolling process, thus providing an opportunity to detect subtle deformation caused by object motion modes by analyzing detailed elastomer deformation (**Figure 1a**).

The recognition of detailed and subtle deformation requires the system to have the characteristics of large information content and high resolution. The optical image perception-based method can meet this demand.[42] Our previous research has constructed an optical system that can effectively visualize and digitize the surface morphology of elastomers (Figure S1, Supporting Information).[43] Within the field of view, the morphology of the elastomer surface and the small variations in time are continuously encoded and transmitted by the optical signals. The CMOS in the system is to record elastomer deformation information encoded using optical signals that are directly related to the kinematic patterns of the objects that are interacting with the contact. As a form of storing motion patterns, the distribution of pixels on an image contains key features for resolving motion patterns. Parallel light incidence and reflection in the deformation region allow the optical image to faithfully record the state of deformation produced on the elastomer, thus allowing the sphere's behavior to be determined by the different deformations caused by various motions (Figure 1b). For example, when a sphere slides on the PDMS, the elastomer deforms to a greater degree in the front side of the motion direction. Under the interaction of contact stress, the curvature of the elastomer surface profile on the rear side of the movement direction tends to be flat, which is manifested as a smaller surface deformation angle and a larger deformation area. It results in asymmetric deformation of the elastomer.[38–40] This asymmetric deformation will result in dynamically changing optical image features. The evolution characteristics of the elastic medium surface profile are tiny in the image. Thanks to the local feature extraction capability and positional non-specificity of convolutional neural networks, the characterization of optical images can accurately and dynamically identify individual positional features recorded on optical images and analyze the movement pattern of the sphere in real-time. (Figure 1c).[44–47]

Since the contact behavior is recorded by optical images, it is necessary to discuss the relationship between the contact state and the image pixel distribution to accurately identify the spherical motion. **Figure 2a,b** shows that the elastomer will occur two different deformations during the sphere rolling and sliding. The sphere is pressed with a vertical load to ensure its contact with Polydimethylsiloxane (PDMS). A horizontal force is applied on the sphere in a contact state to produce uniform velocity. This process is discussed through direct experimental observations that are presented in Figure S2 (Supporting Information). When the elastomer is pressed by a sphere vertically, it deforms and conforms to the shape of the sphere, which enables its close contact with the sphere. As a horizontal force is applied to the sphere in contact, the sphere moves horizontally on the elastomer, causing further deformation of the elastomer and partial loss in conformability. This dynamic process directly affects the evolution of the surface profile of the elastomer over time (Figure 2c). Such movement changes during this contact can be fully presented and recorded in the optical system. Since both the elastomer deformation and the light transmission are continuous, the resolution of the variation produced in tiny areas depends on the spacing of the receiving units where the sampling is performed. The large number of dense pixels on CMOS

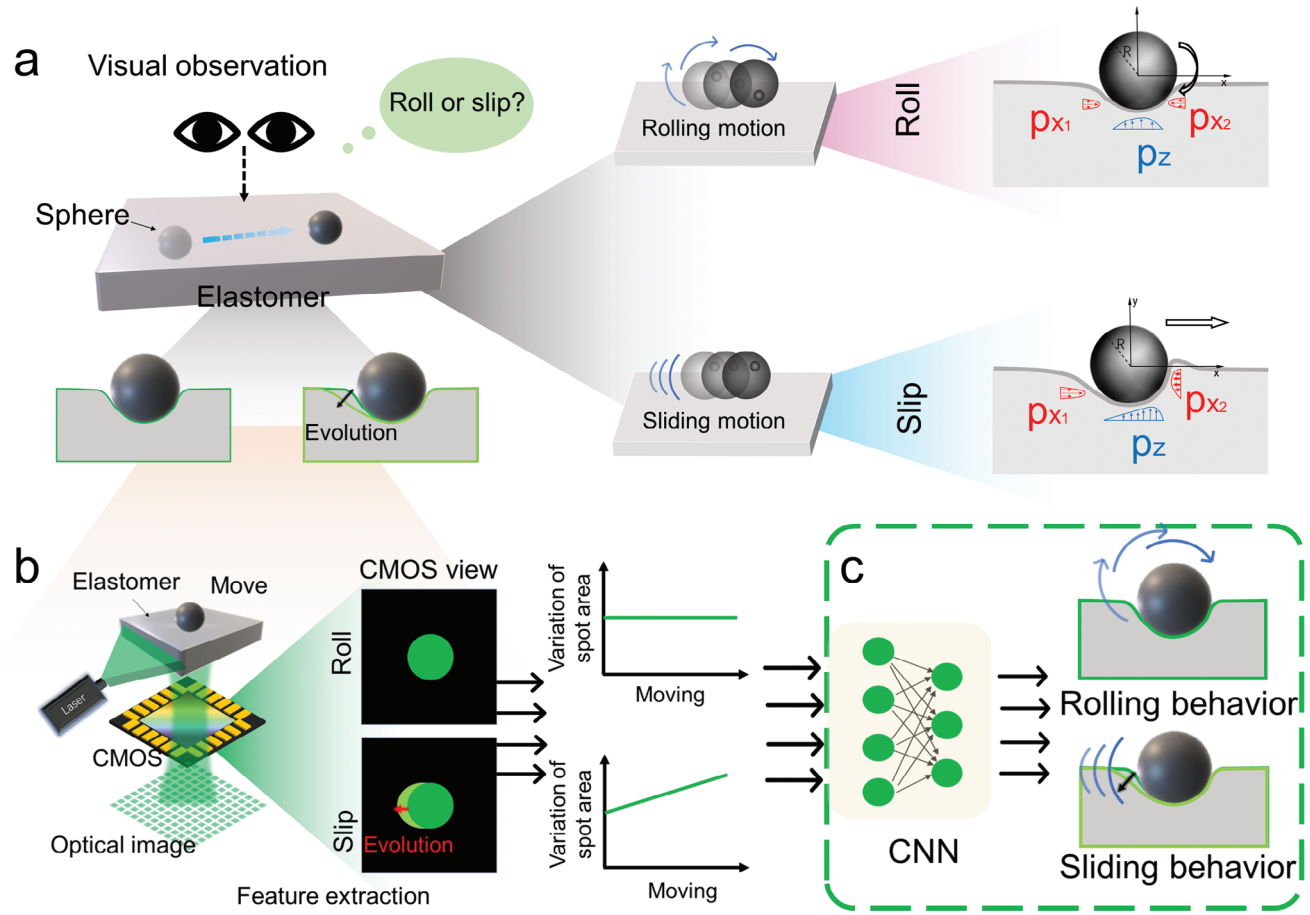

Figure 1. Optical detection method for dynamic subtle deformation of elastomer surface. a) Symmetric and asymmetric deformation of elastomer when the sphere moves. P_z: Vertical contact stress P_{x1}, P_{x2}: Horizontal contact stress. b) The scheme of recognition system of sphere motion modes. c) The motion modes recognition with CNN in real-time.

enables the dynamic visualization and digitization of the elastomer surface profile change process in real-time (The experimental procedure refers to "slide and roll tests" of Methods). Further, the minute changes in elastomer deformation presented by the pixels enable the reflection of minute responses that are sufficiently fine.

As shown in Figure 2d, the PDMS generates symmetric deformation around the contact region in the rolling process (Video S1, Supporting Information). As shown in the top view, the symmetrical deformation lies right below the sphere and cannot be observed directly. The optical image appears as a circular light spot. With a sliding sphere, the elastomer surface has additional deformation on the rear side of the sphere's motion direction in the top view (Video S2, Supporting Information). The asymmetric deformation of the elastomer surface enables the increase of the light reflection area and results in more CMOS pixel units to respond to the reflected light signal. In optical images, this dynamic process is recorded as a crescent "drag" shape area gradually increasing from nothing (Figure 2d). In addition to the sphere's motion along the x-axis of the image field of view, this phenomenon could be observed in other motion directions (Figure S3, Supporting Information).

2.2. Analysis of Image Features of Deformation During Sphere Movement

To further understand the dynamic motion characteristics of the sphere through soft interface deformation, it is necessary to digitally analyze the evolution process of the surface profile. We extract the spot area from the images and the variation of the spot area S/S_0 during the motion, where S_0 represents the spot area when the object is static and S represents the spot area at any time during the motion. In addition, to gain a sensible insight into the impact of sphere sliding on image features, a new feature parameter L is introduced to represent the length of the elastomer surface deformation in the direction of motion, expressed in pixels. The optical system records the dynamic surface profile evolution process caused by sphere sliding and rolling at a speed of 0.5 mm s^{-1} in **Figure 3a** (i, ii). The influence of the different motion behaviors of the sphere on the surface profile of the elastomer could be characterized by the variation in the size of the image feature area. The result of this dynamic change could be evaluated by image features and channel value distribution (Figure 3a (i, ii)). We further discuss the relationship between the movement speed of the sphere and the variation of image features (displacement distance is 1.5 mm, refer to Figure 3b).

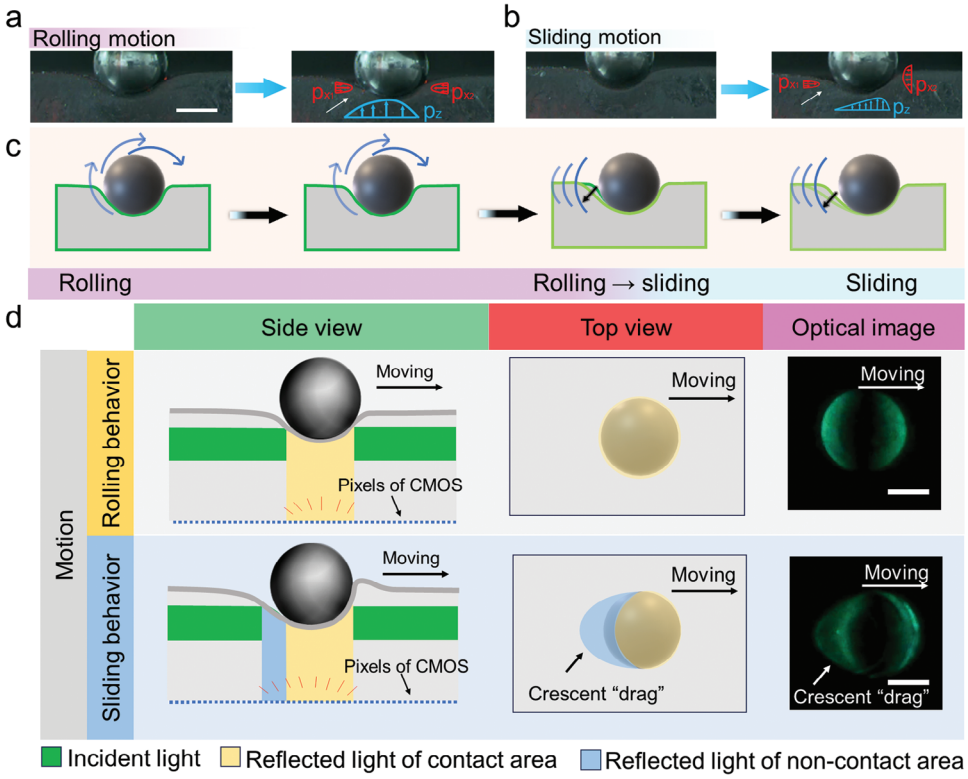

Figure 2. Optical image features of subtle deformation caused by the dynamic motion of the sphere. a) The sphere rolls on the surface of the elastomer, resulting in a symmetric deformation of the elastomer. Scale bar, 2 mm. b) The sphere slides on the surface of the elastomer, resulting in an asymmetric deformation of the elastomer surface. c) Evolution of elastomer surface profile during sphere moving. d) Interface deformation and optical images under different motion behaviors. Scale Bar, 1 mm. The side view and top view are schematic diagrams of the sphere moving on the elastomer.

The results show that the area does not vary significantly at different speeds when the sphere rolls. Compared with the rolling behavior, the sliding speed of the sphere affects the rate of change of the image area, which is manifested as a positive correlation between the rate of change of the elastomer surface deformation area and the sliding speed.

Notably, the growth rate of the "drag" area can be correlated with the movement velocity of the sphere. Figure 3c shows the evolution process of this image feature in the form of a schematic diagram. For the sphere sliding over the elastomer, after the sphere reaches a certain displacement, the size of the "drag" area is correlated with the motion velocity (Figure 3d; Figure S4, Supporting Information). This is probably related to the hysteresis of elastomer deformation. The dynamic changes of the optical image features are similar to the deformation trend of the elastomer caused by the sphere movement, showing that the optical system we proposed can realize real-time recognition of sphere motion speed on the deformation of elastic surface to a certain extent.

To further discuss the system's ability to identify the difference of deformation in real-time, we analyze the variation of the image features at each motion moment in an early moving phase (refer to the dynamic acquisition of sphere motion images of experimental procedures). As shown in Figure 3e, the image feature length L (along the movement direction) begins and continues to increase as the movement progresses after the sphere slips for 0.6 s (0.3 mm of displacement distance). For the rolling behavior of the sphere, the image feature length L does not change significantly. Figure 3f shows the distribution of channel value response to the motion behaviors at the time of 2.4, 3.0, 3.6, 4.2, and 4.8 s in the optical image. During the movement of the sphere with a tiny displacement, the image channel value distribution records the slight changes in the surface profile of the elastomer. The results show that at the beginning of the movement, the change rate of the image feature length L is relatively slow at first (displacement less than 0.3 mm), then gradually increases, and finally tends to be stable (displacement more than 0.6 mm and refer to Figure 3g). This phenomenon may be related to the deformation characteristics of the elastomer itself. These observations suggest that in the early stages of the sphere's motion, the image features of its sliding behavior may be difficult to distinguish from the image features of its rolling behavior. The above results show that the optical recognition method we proposed can dynamically capture the elastomer surface profile caused by the movement behavior in real-time.

The image characteristics of the subtle elastomer deformation caused by sphere sliding are represented by tiny features contained in each pixel area. The convolutional neural network (CNN) can effectually perceive and extract these global and local features, and then for recognition and judgment (**Figure** 4a). During the dynamic movement of the sphere, the elastomer surface deformation recorded in real-time by CMOS is input into CNNs for behavior classification (refer to the dynamic acquisition of sphere motion images of experimental procedures). The result shows that the recognition rate of sliding motion modes

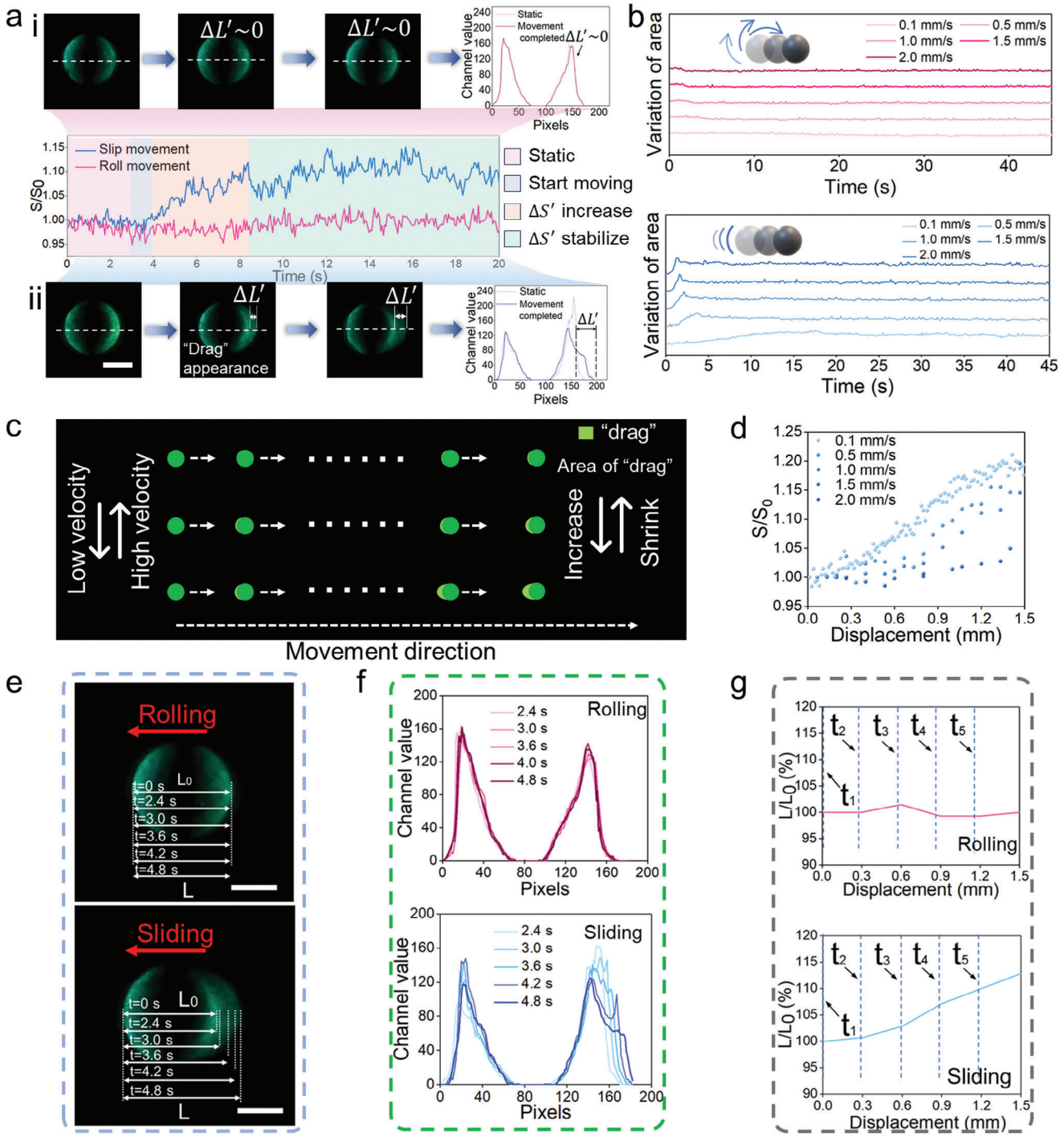

Figure 3. The variation of area and sphere motion. Scale Bar, 1 mm. a) (i) Sphere moves on PDMS with 0.5 mm s^{-1} velocity, variation of "drag" width for sphere rolling. (ii) Sphere moves on PDMS with 0.5 mm s^{-1} velocity, variation of "drag" width for sphere sliding. b) The relation between the variation of the spot area and the velocity during rolling and sliding motions. c) Schematic diagram of the change of optical image characteristics at different sliding speeds of the sphere. d) The effect of sliding velocity on variation of area. e) The change process of optical image feature under small displacement distance. f) The distribution of image channel values corresponds to the two motion behaviors under small displacement. The data sampling is at t = 2.4, 3.0, 3.6, 4.2, and 4.8 s respectively) The change process of image feature length L under a small displacement distance. Where t_1, t_2, t_3, t_4, t_5 represents time equal to 2.4, 3.0, 3.6, 4.2, 4.8 s.

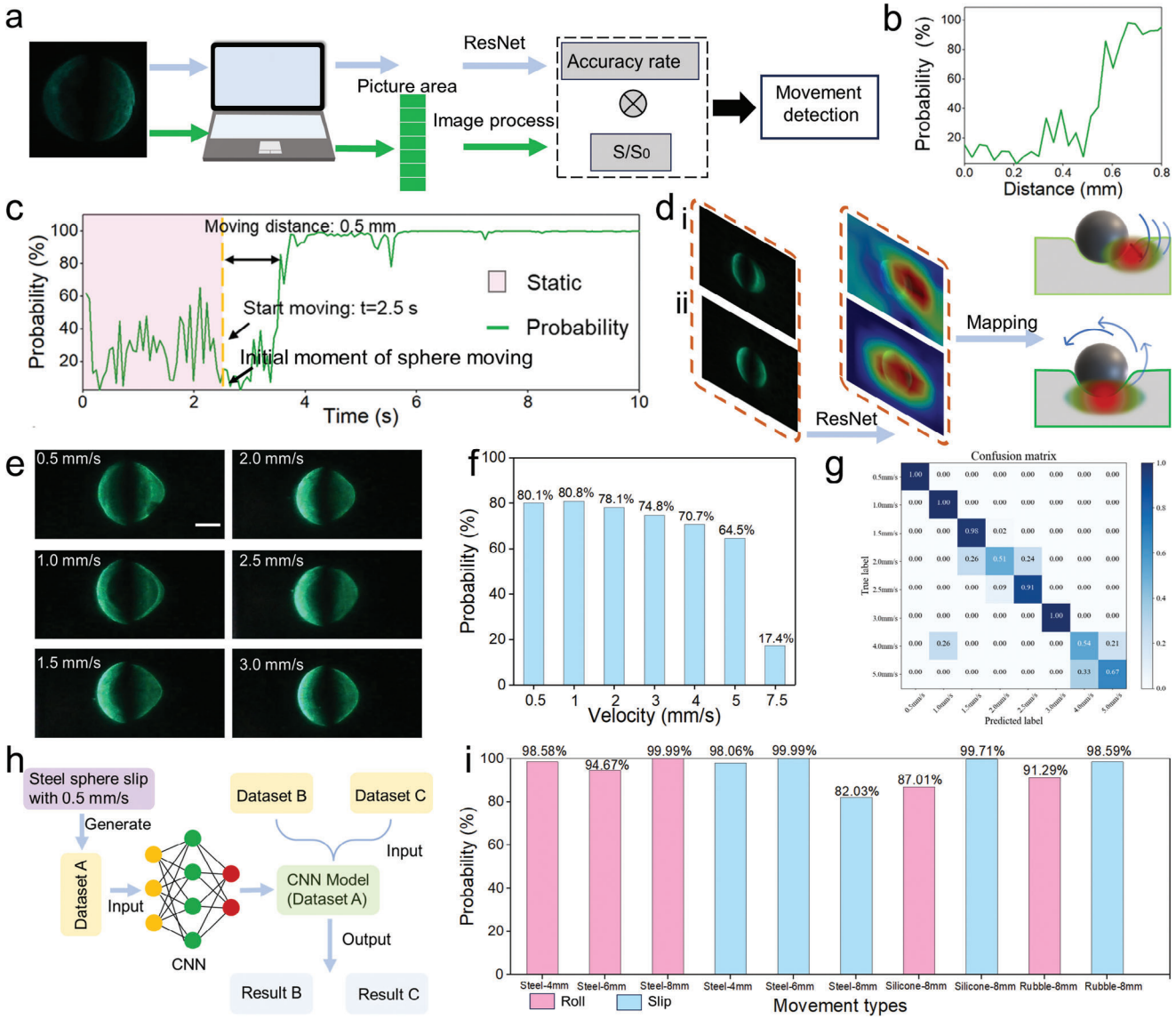

Figure 4. Dynamic effects of motion behavior on algorithm recognition probability. Scar bar, 1 mm. a) The strategy of sphere motion modes recognition. b) The variation of the area under different motion displacements and recognition accuracy were obtained by using CNN. c) variation of identification accuracy during the sphere sliding process. d) Neural network heat map. Scale Bar, 1 mm. (i) Image and heat map of rolling motion. (ii). Image and heat map of sliding motion. e) The optical images of a sphere moving at the same displacement at different velocities. f) The result of CNN's probability of recognizing sliding behaviors during sphere sliding with different velocities. g) The ability of CNN to distinguish spheres move at different velocities. h) The framework for model robustness verification. i) The result of model robustness verification, the shore hardness of steel sphere, rubber sphere, and silicone sphere are 90, 75, and 70 respectively.

shows a trend of increasing with the movement process, and finally stabilizes above 90%. It indicates that our proposed idea of using deformation characteristics for motion recognition is feasible (Figure 4b). Figure 4c shows the change in the accuracy of CNN in classifying the motion modes of the sphere during the early stages of spherical motion. The recognition probability curve of sliding behavior shows that it rises rapidly as the movement progresses and finally maintains a high level. When the 6 mm diameter sphere moves only 8.3% of its diameter distance (0.5 mm), the CNN's motion pattern recognition accuracy reaches 80%. However, it is worth noting that in the early stage of the sphere's movement, the recognition probability of the movement behavior has remained at a low level (less than 40% as shown in Figure 4b). When the movement displacement reaches a certain threshold (0.45 mm as shown in Figure 4b), the recognition probability of the CNN for the movement behavior rises sharply. This phenomenon may be consistent with the results discussed in Figure 3g, that is, in the early stage of the sphere's movement, the image features of subtle elastomer deformation caused by its rolling behavior are difficult to distinguish from the image features of its sliding behavior, which affects the recognition probability output by the CNN.

The contribution of image features to motion recognition can be explained by neural network heatmaps (Figure 4d). The heat

map shows that the neural network mainly focuses on the overall pattern feature for the sphere rolling images (Figure 4d (i)). Compared with the rolling moving image, the "drag" feature in the sliding moving image shows higher attention, which indicates that the image with the "drag" feature is easier to classify as sliding motion (Figure 4d (ii)). This shows that the elastomer deformation feature related to sphere motion behavior is the key factor in realizing motion pattern recognition.

It is worth noting that the association between the sphere's speed and the "drag" feature affects the accuracy of the algorithm in distinguishing movement patterns. Figure 4e shows an optical image of a sphere with a diameter of 6 mm moving 10 mm, which contact with the surface of an elastomer at a constant pressure. When the sphere moves in contact with the elastomer at a constant normal pressure, the proportion of the "drag" feature in the overall image features is inversely proportional to the velocity of movement (Figure S4, Supporting Information). In addition, Due to the limitation of CMOS performance, the excessively fast movement speed causes blurred ghosting in the image (Figure S5, Supporting Information), resulting in a rapid decrease in the accuracy rate of CNN's to distinguish rolling and sliding behaviors. This phenomenon affects the recognition of rolling and sliding behaviors by the CNN algorithm. The faster the sphere moves, the lower the probability of correctly identifying the sliding behavior (Figure 4f). The reason for this phenomenon may be related to the deformation characteristics of the elastomer and the CMOS frame rate. When the speed of the sphere increases, the creep characteristics of the elastomer cause the surface deformation behavior to lag behind the movement of the sphere. This is manifested in that when moving the same distance, the size of the "drag" feature is inversely proportional to the speed of movement, which reduces the accuracy of CNN's distinction of motion behavior. When the speed of the sphere exceeds a certain threshold, due to the limitations of the CMOS frame rate and exposure time, the moving image will appear ghosting and blurring. This makes it impossible for CNN to accurately identify the movement behavior. In particular, the optical system proposed in this work has a detection limit of $\approx$5 mm s^{-1} for the speed of the sphere. In addition, we also explored the system's ability to identify the velocity of the sphere. Within the selected speed range, the average accuracy of CNN classification for any frame optical images reaches 82.7% (Figure 4g). This shows that it is possible to analyze dynamic motion information from static optical images.

In addition to the speed of movement, some physical parameters of the sphere during movement may affect the elastomer surface's subtle deformation, to change the image features, thereby affecting the performance of the algorithm in identifying motion behavior. For example, load applied on the sphere, hardness of the sphere, and other factors (Figures S6–S8, Supporting Information). In particular, a sphere with too low hardness cannot produce significant elastic deformation, which ultimately affects the recognition of motion behavior. The size of the sphere affects the minimum relative motion displacement distance required for the system to accurately identify the motion pattern. Therefore, it should take into full consideration the physical properties related to objects when discussing the image features to motion modes recognition ability. Since the size, material and other parameters of the sphere will affect the recognition ability of the system, it is necessary to explore the robustness of the method. First, a steel sphere with a diameter of 6 mm is used to collect motion images at a speed of 0.5mm s^{-1} to construct a data set. CNN will generate a motion recognition algorithm model through this data set. Other data sets that have not been trained by CNN are sent to the model for rolling and sliding recognition, and finally, an identification result is output (Figure 4h). The result shows that the algorithm has a high recognition probability for the motion behavior of spheres of different materials and sizes, without retraining the neural network for the sphere size and hardness parameters. The reason is that the system's ability to distinguish between movement modes is conditional on the system's ability to capture tiny differences in elastomeric variables resulting from various movement modes and to be able to effectively differentiate them in the algorithm. Thus, our method can be used to directly discriminate between spheres of different hardness and size interacting with the elastomer whenever the state of motion causes the elastomer to change concerning the motion pattern. For a neural network that has learned pattern difference features for one type of sphere, the feature differences induced by different hardnesses and sizes of spheres are in the same feature framework, thus the conditioning factors used for pattern recognition can be migrated to different spheres (Figure 4i). Meanwhile, it is worth noting that the applicability of the same neural network has a limited range, considering the nature of the elastomer and the inconsistency in the type of features produced by the motion patterns of different objects. In the experiments, this difference in applicability is reflected in the variation of prediction probabilities.

2.3. Dynamic Real-Time Recognition of Deformation Application Scenarios

Interactions in physical space are often guided and driven by relative motion trends that exist before the motion occurs. Obtaining this motion tendency before the actual motion begins can help determine the state of an object and predict possible motion events. Behavior-based motion data can be encoded by the system into quantifiable tactile signals, which can be used as constraints or judgment methods to participate in the construction of digital bionic physical models, providing support for digital twins technology and tiny physical interactive behaviors For example, if a person stands on the ground and wants to move, he needs to apply force to the ground. At this time, there is an interaction relationship on the interactive interface that represents this motion trend. Recording and identifying such movement trends facilitates the encoding and decoding of interaction instructions.

Here, we take "behavior prediction" as an example to demonstrate this application prospect with a 3D-printed leg model (**Figure 5a**). The initial contact contour between the "foot" and the elastic interface is represented by the red trajectory. As the horizontal driving force increases, the leg model goes through three stages: "stand" to "try to move" to "moving". In the "try to move" stage, the leg model moves to the right with a tiny distance and keeps relatively stationary with the elastomer surface in the inertial reference frame. In this stage, it does not appear to move visually. However, the appearance of the "drag" feature has been captured in the optical image, indicating that the "leg" is driving the elastic surface to slide (Figure 5b; Video S3, Supporting

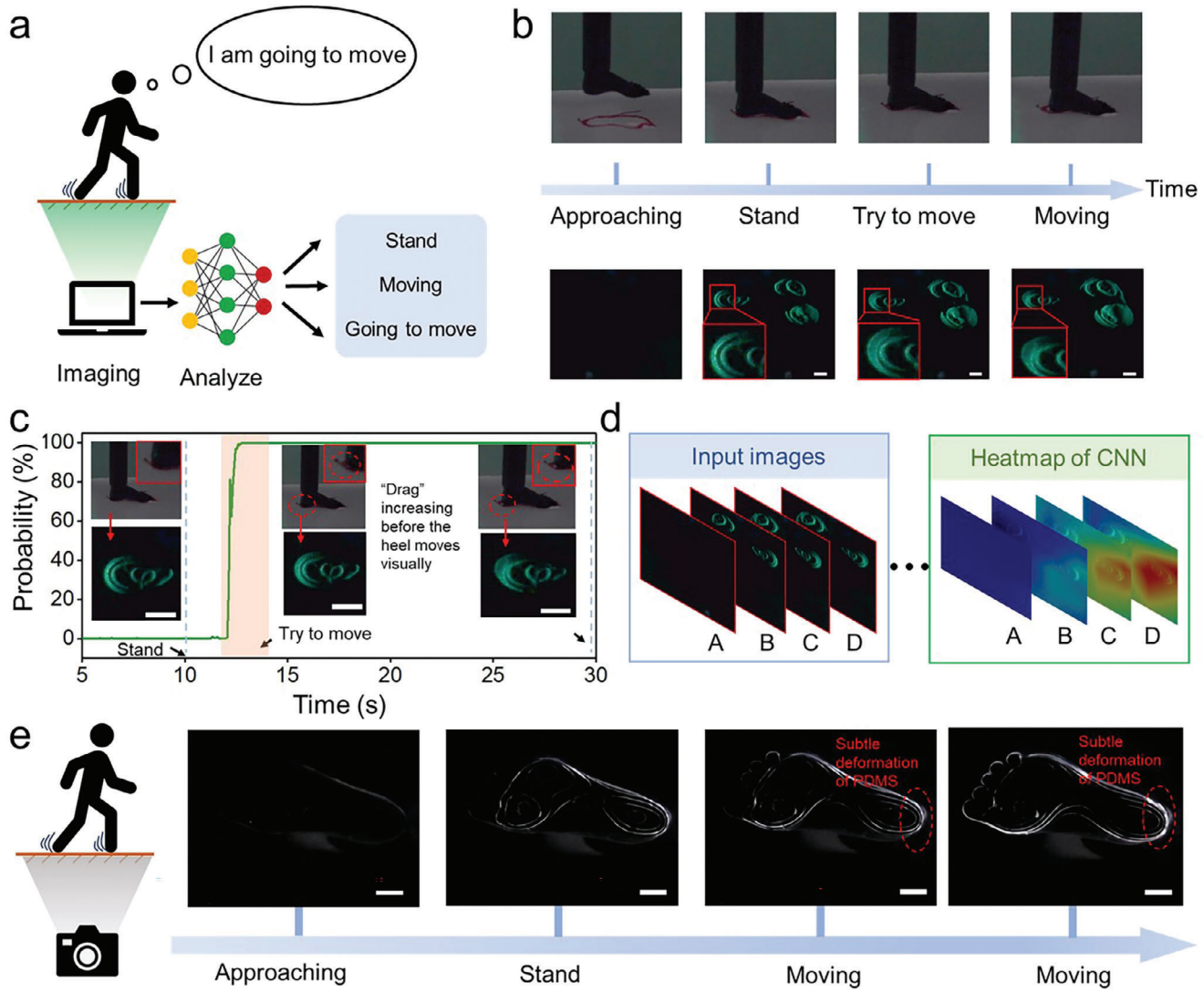

Figure 5. Demonstration of "prediction of behavior". Scale Bar, 0.5 mm. a) The schematic diagram of the prediction system for analysis of optical images. b) The process behavior from approaching to moving "feet" with images. c) The system recognizes the relative movement of the "feet" before it is visually detected. d) The CNN net calculates the image feature that contributes to motion behavior prediction. e) The process of "feet" from approaching to move captured by the camera directly.

Information). In addition, as the driving force increases, the size of the deformation feature is gradually bigger. The appearance of the image feature occurs before the relative motion occurs, indicating that the method based on the detection of subtle contact interface deformation has a certain potential in behavior prediction. The relationship between the probability of identifying the "try to move" behavior and time also supports this conclusion (Figure 5c). In addition, the heat map of the convolutional neural network shows that the "drag" feature of the heel area in the optical image plays a major role in motion recognition (Figure 5d), indicating that the small deformation in contact interface caused by the motion trend plays a key role in the recognition of motion behavior. To intuitively illustrate the evolution of the elastic interface in this process, Figure 5e shows the contact process between the leg model and the PDMS interface captured directly by CMOS. In addition, the system's ability to dynamically image elastic deformation has the potential to be applied to scenarios that are sensitive to motion behavior, such as writing and erasing (Figure S9 and Video S4, Supporting Information).

When faced with more complex interaction scenarios, the limited number of codes that accurately and effectively represent each type of information may be limited. The behavior present in each person's movement patterns and gestures is a way of encoding information that depends on the individual. When we can distinguish movement patterns and use the movement behavior during the input process, rather than just the result of the input, as the source of information, a richer source of available data can be generated in a limited process. The addition of pattern recognition can achieve differentiation by presenting the habits of different people, even if the interaction time and space are short. This is difficult to achieve by only observing the results of the

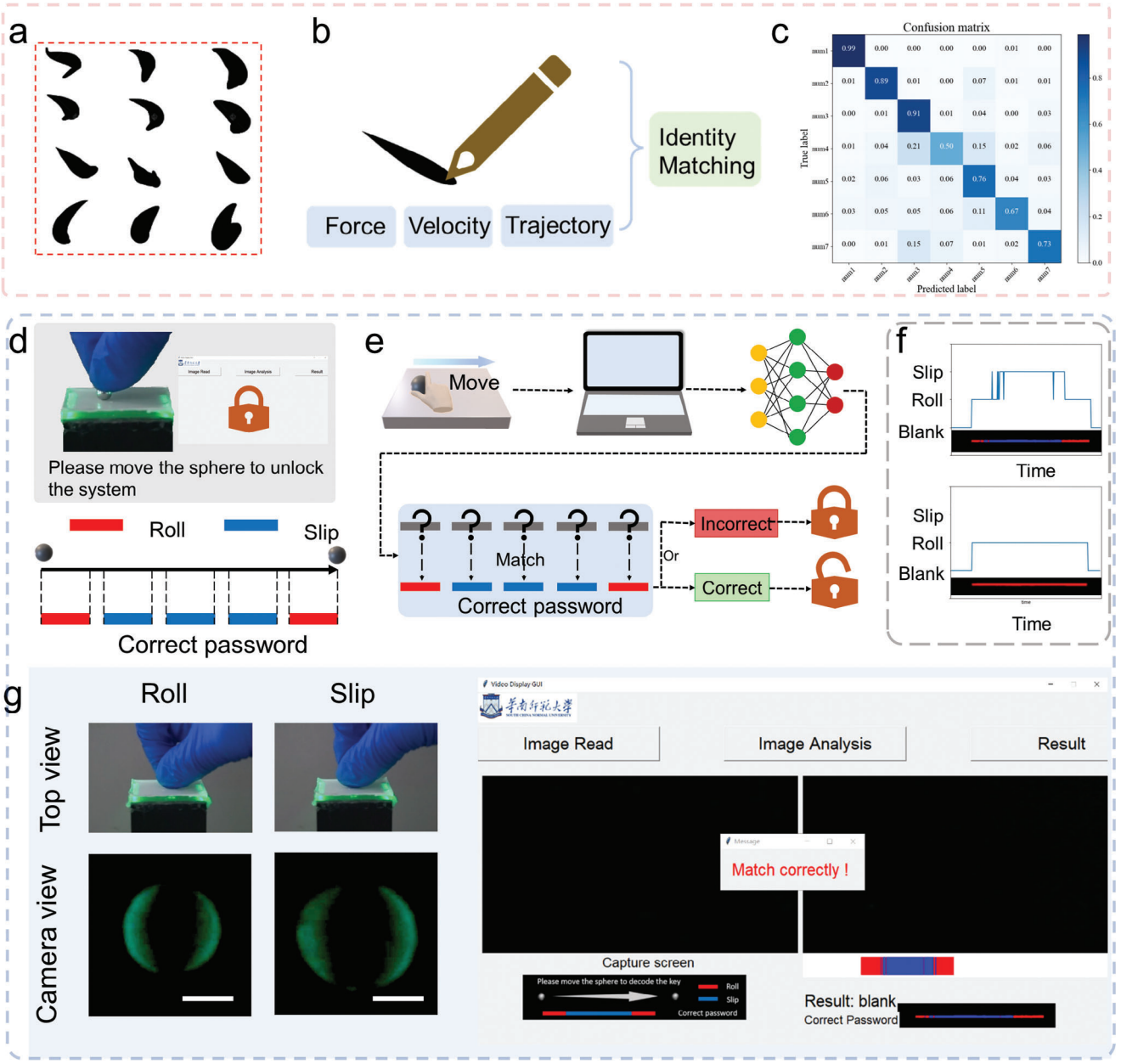

Figure 6. Behavioral encryption in human-computer interaction system. Scale Bar, 1 mm. a) Different fonts for symbols. b) The writer's identification strategy based on the distribution of force, speed, and trajectory in writing habits. c) The results of CNN for identifying different writers. d) Unlocking the system by moving the sphere. e) Schematic diagram of the system unlocking process. f) Motion recognition results of the unlocking process. g) Demonstration of the unlock process.

interaction. We discuss this idea by distinguishing information encryption with process differences. Using the ability to visualize the evolution of interface subtle deformations during contact dynamics, we developed an ML framework that can distinguish the identity of individual writers. Due to the different writing habits of each person, the force, speed, and trajectory are different when writing the same symbol or word (**Figure** 6a). The coherence of these physical parameters will cause a unique evolution of interface deformation features. Visualizing and digitizing this feature can identify the writer (Figure 6b). The neural network can recognize the handwriting of different writers with an accuracy rate of 77.9% (Figure 6c).

The fact that movement habits are encoded in the data traces and can be recognized can be used for encryption and decryption of the information. Data input steps may be used to decrypt encrypted messages, but introducing different state modes as additional variables in the motion process of the same path can make the process less susceptible to decryption. This process can be realized by introducing movement behavioral characteristics into cryptographic systems to encryption, and decode it by

recognizing these dynamic motion features with slight differences. To demonstrate this concept, a sliding unlock scene is proposed. When a system needs to be unlocked, it should first need to control the "decoder"—the sphere to move (Figure 6d). During the movement of the sphere, the movement behavior needs to be changed and recorded in real-time. (The red and blue represent the rolling and sliding of the sphere respectively. (Figure 6e)). The moving images of the sphere are fed into a convolutional neural network for training and classification, then compared with preset motion patterns, and finally the motion type of each image is output. When the motion modes are consistent with the preset results, the system is unlocked successfully (Figure 6f). Figure 6g shows the recognition results of the correct permutation of motion modes and the incorrect permutation of motion modes (Recognition probability rate refer to Figures S10 and S11, Supporting Information). The external view and camera view of the decoding process are shown in Figure 6g. The recognition rate of the neural network for the motion modes is 77.7% when the sphere is switching motion behavior. The recognition rate of the neural network for the motion modes is 98% when the sphere is stably rolling or sliding. We demonstrated this process in the Graphical User Interface (GUI) unlock scene (Figure 6g; Video S5, Supporting Information).

3. Conclusion

To recognize the motion-induced micro-deformation on the elastomer's surface and their disappearance during time-lapse, this work presents a new scheme of real-time motion mode recognition using an optical tactile sensing system to visualize and distinguish tiny variations in surface profile evolution encoded as images. The deformation features of the elastomer caused by the movement of the sphere are recorded by the imaging system and represented as the geometry of pixels in the optical image. The difference in elastomer deformation between the sliding and rolling behavior of the sphere is rendered by the crescent-shaped "drag" characteristic of dynamic sliding and is shown to be feasible for prediction in conjunction with neural networks. Using high-resolution coding results and feature variations in the optical image reflecting the motion behavior, to achieve the motion state recognition with 80% accuracy when a displacement of only 8.3% of the sphere diameter distance is produced. Its advantage in real-time dynamic visualization and digitization of the deformation evolution of the elastomer surface profile helps to understand the motion behavior of objects through soft interface deformation. In addition, we demonstrated its application in real-time dynamic recognition of sports behavior by building two interactive scenarios: "prediction of motion behaviors" and "behavior encryption." This dynamic micro-deformation recognition framework based on image recognition provides the value of input command recognition based on motion behavior design in human-computer interaction. This system is expected to be applied to digital twin technology and to guide the construction of real physical interaction patterns in simulation. By encoding behavioral operations in the real physical world, objects in the virtual digital world can be operated. It has development prospects in the fields of human-computer interaction and augmented reality (AR)/ virtual reality (VR).

4. Experimental Section

System Design: The incident light irradiance was 70.27 lx. The spatial line width was 1.5 mm, and the distance from the sample was 100 mm. The CMOS module was a Logitech G270 camera with a resolution of 1280 × 720 and a video frame rate of 16 Hz. The sensor structure refers to Figure S12 (Supporting Information).

Slide and Roll Tests: The elastomer used in the experiment was A PDMS with a cross-linking ratio of 10:1. A steel sphere with Shore hardness A of 90 HA and a diameter of 6 mm was selected for the sample. The sphere was fixed on the dynamometer adapter, and the sliding motion was driven by the cylindrical rotor of the dynamometer. The rolling motion was driven by the disc-type adapter, and there was no fixed treatment between the sphere and the adapter. The driving mode of the sphere and the deformation of the elastomer surface caused by sphere movement refer to Figure S13 (Supporting Information). A 7 N load was first applied to a steel sphere with a diameter of 6 mm. Then the sphere was given different velocities to make it move horizontally. After a normal load of 7 N was applied, the steel ball was driven by a horizontal displacement table to slide and roll at a speed of 0.1, 0.5, 1.0, 1.5, 2.0 mm s^{-1} (in the sliding test, The displacement distance of the center of the sphere was equal to the horizontal displacement of the displacement table. In the rolling test, the displacement distance of the sphere center was equal to half of the horizontal displacement of the displacement table).

Spot Area Calculation: Spot area was calculated by cumulative method to calculate the number of pixels in any frame image whose G channel value was greater than 5 (due to hardware problems, a single pixel in the image will produce 0–3 channel value fluctuations), and the sum of all pixels in an image that meets this condition was the area of the spot in the image.

CNN Configuration in the Experiment: Before neural network training, data enhancement operations were first performed on the images. The pattern was translated and rotated randomly, and the noise was added randomly. The ResNet50 network was used to calculate the result. The official pre-model was loaded. The data set was divided into training set, verification set, and 0.6:0.2:0.2 test set. Each experimental group trained 80 epochs with a learning rate of 0.01. The lowest weight setting loss value was verified during the experimental selection training.

Dynamic Acquisition of Spherical Motion Images: A sphere with a diameter of 6 mm was subjected to a normal load of 7 N. Driven by the adapter, the sphere moved at a constant speed of 0.5 mm s^{-1}. The moment when the CMOS starts to collect images was taken as time zero moment. The sphere started to move at t = 2.4 s. The CMOS records 16 fps per second.

Recognition of "Write" and "Erase": The convolutional neural network classifies a circle pattern as a "rolling behavior." Then the system recognizes this instruction as "writing" and will read the spot position of the current frame number image. Due to the translation invariant nature of the neural network, the position of the pattern in the image does not affect the judgment of the type of motion. When images with consecutive frames were recognized as rolling, the system will record the position of the spot in the continuous frame image as a continuous writing track. When the slip terminal of the pen moves, the "drag" begins to appear on the rear side of the circle pattern. The "drag" will become more pronounced as the increase of the distance pen moves. The convolutional neural network classifies it as "sliding behavior". Then the system recognized the instruction as "erase" and records the spot position of the current frame number image.

Supporting Information

Supporting Information is available from the Wiley Online Library or from the author.

Acknowledgements

Z.B.Z. and Z.L.L. contributed equally to this work. X.M.L. acknowledges the financial support from the Guangdong Basic and Applied Basic Research

Foundation (No. 2022A1515010136), the Guangdong Provincial Key Laboratory of Nanophotonic Functional Materials and Devices, and the South China Normal University start-up fund. The authors thank Erteng Chen from Peking University, Zefeng Chen from South China Normal University, Ming Zhou from Guangxi University of Science and Technology, and Tingting Yang from Southwest Jiaotong University for the discussions.

Conflict of Interest

The authors declare no conflict of interest.

Data Availability Statement

The data that support the findings of this study are available from the corresponding author upon reasonable request.

Keywords

dynamic recognition, microscale deformations, optical imaging, visualizing surface profiles

Received: September 8, 2024
Revised: November 21, 2024
Published online: December 6, 2024

[1] X. Xiao, J. Wang, P. Feng, A. Gong, X. Zhang, J. Zhang, *Nat. Commun.* **2024**, *15*, 2423.
[2] J. Zhang, Z. Jin, G. Chen, J. Chen, *Microsyst. Nanoeng.* **2024**, *10*, 109.
[3] R. Han, Y. Liu, Y. Mo, H. Xu, Z. Yang, R. Bao, C. Pan, *Adv. Funct. Mater.* **2023**, *33*, 2305531.
[4] Y. Wang, J. Liang, J. Yu, Y. Shan, X. Huang, W. Lin, Q. Pian, T. Zhang, Z. Zhang, Y. Gao, X. Yu, L. Wei, Z. Yang, *Device* **2024**, *2*, 100326.
[5] X. Wu, X. Luo, Z. Song, Y. Bai, B. Zhang, G. Zhang, *Adv. Funct. Mater.* **2023**, *33*, 2303504.
[6] J. Ge, X. Wang, M. Drack, O. Volkov, M. Liang, G. S. C. Bermúdez, R. Illing, C. Wang, S. Zhou, J. Fassbender, M. Kaltenbrunner, D. Makarov, *Nat. Commun.* **2019**, *10*, 4405.
[7] X. Xu, K. Scott, J. Chen, *Device* **2024**, *2*, 100462.
[8] J. Zhang, X. Hou, S. Qian, J. Huo, M. Yuan, Z. Duan, X. Song, H. Wu, S. Shi, W. Geng, J. Mu, J. He, X. Chou, *Microsyst. Nanoeng.* **2024**, *10*, 64.
[9] J. Kang, J. Yoon, B. Lee, H. Jung, J. Kim, W. Nam, K. Jeong, J. Choi, D. Son, S. G. Im, *Device* **2024**, *2*, 100426.
[10] D. B. Kim, J. Han, S. M. Sung, M. S. Kim, B. K. Choi, S. J. Park, H. R. Hong, H. J. Choi, B. K. Kim, C. H. Park, J. H. Paik, J.-S. Lee, Y. S. Cho, *npj Flexible Electron.* **2022**, *6*, 69.
[11] J. Qu, G. Cui, Z. Li, S. Fang, X. Zhang, A. Liu, M. Han, H. Liu, X. Wang, X. Wang, *Adv. Funct. Mater.* **2024**, *34*, 2401311.
[12] D. Zhao, Y. Zhu, W. Cheng, G. Xu, Q. Wang, S. Liu, J. Li, C. Chen, H. Yu, L. Hu, *Matter* **2020**, *2*, 390.
[13] H. Sun, G. Martius, *Sci. Rob.* **2022**, *7*, eabm0608.
[14] X. Han, X. Wu, L. Zhao, M. Li, C. Jia, Z. Li, J. Xie, G. Luo, P. Yang, R. Boukherroub, Y. Türker, M. U. Özkaynak, K. B. Dönmez, *Microsyst. Nanoeng.* **2024**, *10*, 107.
[15] R. Del-Rio-Ruiz, D. R. R. Silva, H. Suresh, H. Asci, D. M. Santos, A. Sharma, G. Widmer, S. Sankusale, *Device* **2024**, *2*, 100406.
[16] Y. Zhou, W. Xu, Y. Ji, G. Zhou, W. Wu, Z. Chen, B. Wang, X. Gui, X. Li, *Appl. Phys. Rev.* **2023**, *10*, 021407.
[17] A. Leber, C. Dong, R. Chandran, T. D. Gupta, N. Bartolomei, F. Sorin, *Nat. Electron.* **2020**, *3*, 316.
[18] H. Jin, Y. Kim, W. Youm, Y. Min, S. Seo, C. Lim, C.-H. Hong, S. Kwon, G. Park, S. Park, H. J. Kim, *npj Flexible Electron.* **2022**, *6*, 28.
[19] V. Adepu, C. Yoo, Y. Jung, P. Sahatiya, *Appl. Phys. Lett.* **2023**, *122*, 263505.
[20] A. Georgopoulou, D. Hardman, T. G. Thuruthel, F. Iida, F. Clemens, *Adv. Sci.* **2023**, *10*, 2301590.
[21] J. R. Barber, *Contact Mechanics*, Springer, Berlin, Germany **2018**.
[22] K. N. Calahan, Y. Qi, K. G. Johannes, M. E. Rentschler, R. Long, *Sci. Adv.* **2022**, *8*, eabn2728.
[23] Y. Zhao, B. Zhang, B. Yao, Y. Qiu, Z. Peng, Y. Zhang, Y. Alsaid, I. Frenkel, K. Youssef, Q. Pei, X. He, *Matter* **2020**, *3*, 1196.
[24] C. Lin, H. Zhang, J. Xu, L. Wu, H. Xu, *IEEE Robot. Automat. Lett.* **2024**, *9*, 923.
[25] S. Zhu, P. Wu, H. Yelemulati, J. Hu, G. Li, L. Li, Y. Tai, *Matter* **2021**, *4*, 1838.
[26] W. Lin, B. Wang, G. Peng, Y. Shan, H. Hu, Z. Yang, *Adv. Sci.* **2022**, *8*, 2002817.
[27] C. Xu, Y. Yang, W. Gao, *Matter* **2020**, *2*, 1414.
[28] S. Li, X. Chen, X. Li, H. Tian, C. Wang, B. Nie, J. He, J. Shao, *Sci. Adv.* **2022**, *8*, eade0720.
[29] C. Liu, Z. Huang, S. Huang, Y. Zhang, B. Li, F. Nan, Y. Zheng, *ACS Nano* **2024**, *18*, 19391.
[30] Q. Wang, M. Li, P. Guo, L. Gao, L. Weng, W. Huang, *Microsyst. Nanoeng.* **2024**, *10*, 103.
[31] L. Wijayarathne, Z. Zhou, Y. Zhao, F. L. Hammond, *IEEE Trans. Robot.* **2023**, *39*, 3549.
[32] K. S. Chun, Y. J. Kang, J. Y. Lee, M. Nguyen, B. Lee, R. Lee, H. H. Jo, E. Allen, H. Chen, J. Kim, L. Yu, X. Ni, K. Lee, H. Jeong, J. Lee, Y. Park, H. U. Cheung, A. W. Li, P. A. Lio, A. F. Yang, A. B. Fishbein, A. S. Paller, J. A. Rogers, S. Xu, *Sci. Adv.* **2021**, *7*, eabf9405.
[33] W. Xu, G. Zhou, Y. Zhou, Z. Zou, J. Wang, W. Wu, X. Li, *IEEE Trans. Instrum. Meas.* **2024**, *73*, 5026411.
[34] Y. Li, P. Bai, H. Cao, L. Li, X. Li, X. Hou, J. Fang, J. Li, Y. Meng, L. Ma, Y. Tian, *Nat. Commun.* **2022**, *8*, eabm0984.
[35] S. Hong, V. P. Rachim, J.-H. Baek, S.-M. Park, *npj Flexible Electron.* **2023**, *7*, 30.
[36] N. F. Lepora, A. Church, C. Kerckhove, R. Hadsell, J. Lloyd, *IEEE Robot. Automat. Lett.* **2019**, *4*, 2101.
[37] J. W. James, N. Pestell, N. F. Lepora, *IEEE Robot. Automat. Lett.* **2018**, *8*, 3340.
[38] R. Sui, L. Zhang, T. Li, Y. Jiang, *IEEE Sens. J.* **2021**, *21*, 25973.
[39] D. Baimukashev, Z. Kappassov, *IEEE Robot. Automat. Lett.* **2020**, *5*, 2618.
[40] J. D. Glover, X. Yang, R. Long, J. T. Pham, *Nat. Commun.* **2023**, *14*, 2362.
[41] F. P. Bowden, D. Tabor, *Nature* **1942**, *150*, 197.
[42] P. Zhu, V. A. Papadimitriou, J. E. van Dongen, J. Cordeiro, Y. Neeleman, A. Santoso, S. Chen, J. C. T. Eijkel, H. Peng, L. I. Segerink, A. Y. Rwel, *Sci. Adv.* **2023**, *9*, eadf5509.
[43] Z. Zou, Z. Li, Y. Zhou, G. Zhou, W. Xu, W. Wu, H. Zhang, Z. Chen, Z. Dai, X. Li, *Adv. Intell. Syst.* **2024**, *6*, 2300535.
[44] J. Zhao, Y. Sun, Z. Zhu, J. E. Antonio-Lopez, R. A. Correa, S. Pang, A. Schülzgen, *ACS Photonics* **2018**, *5*, 3930.
[45] Y. Rivenson, T. Liu, Z. Wei, Y. Zhang, K. D. Haan, A. Ozcan, *Light: Sci. Appl.* **2019**, *8*, 23.
[46] F. Wang, C. Wang, C. Deng, S. Han, G. Situ, *Photonics Res.* **2022**, *10*, 104.
[47] C. Son, J. Kim, D. Kang, S. Park, C. Ryu, D. Baek, G. Jeong, S. Jeong, S. Ahn, C. Lim, Y. Jeong, J. Eom, J.-H. Park, D. W. Lee, D. Kim, J. Kim, H. Ko, J. Lee, *Nat. Commun.* **2024**, *15*, 8003.

